Perfect Vortex Modes for Nondestructive Characterization of Mode Dependent Loss in Ring Core Fibers

Mai Banawan, Satyendra K. Mishra, Younès Messaddeq, Sophie LaRochelle, and Leslie A. Rusch

IEEE Journal of Lightwave Technology

Date of Publication: 02 August 2022

Doi: 10.1109/JLT.2022.3195931

https://ieeexplore.ieee.org/abstract/document/9847228

Perfect Vortex Modes for Nondestructive Characterization of Mode Dependent Loss in Ring Core Fibers

Mai Banawan, *Member, IEEE,* Satyendra K. Mishra, Younès Messaddeq, Sophie LaRochelle, *Fellow, IEEE, Fellow, Optica* and Leslie A. Rusch, *Fellow, IEEE, Fellow, Optica*

***Abstract*—Ring core fibers (RCF) enable high-performance modal multiplexing with low crosstalk and can support orbital angular momentum (OAM) modes. RCFs are challenging to characterize due to the lack of commercial multiplexers, especially for high OAM orders. For fibers supporting large numbers of modes, typical cutback techniques for characterization are extremely wasteful of fiber, especially as one cutback is required for each mode. We show the differential modal loss across modes 3 to 10 was significantly underestimated using an OTDR when exciting modes individually or when exciting all modes indiscriminately. We exploit perfect vortex beams to achieve reliable and nondestructive characterization of mode-dependent loss (MDL) for OAM modes. Perfect vortex beams allow us to maximize the coupling efficiency at each mode launch, increasing the accuracy of MDL estimate. We fabricated fiber with a refractive index difference between the ring core and the cladding of a 5.1×10^{-2}. For this fiber, mode orders 3 to 10 are the most suitable for data transmission and were the focus of our work (the fiber support up to OAM order 13). Such a high index difference can lead to MDL. We demonstrate that the modal loss spans from 2.14 to 4.38 dB/km for orders 3 to 10.**

***Index Terms*—Orbital angular momentum (OAM), ring core fiber (RCF), mode-dependent loss (MDL), perfect vortex (PV), mode-division-multiplexing (MDM), time-of-flight (ToF)**

I. Introduction

ORBITAL angular momentum (OAM) modes have attracted significant interest for mode-division-multiplexing (MDM) systems as they reduce multiple-input multiple-output (MIMO) digital signal processing (DSP) complexity [1]. A large modal index separation makes MIMO-free operation more robust to perturbations [2] but increases loss. Ring core fibers (RCFs) for OAM MIMO-free operation are effective over kilometer lengths (suitable within data centers) [1], [3], [4]. In addition to large index separation, the higher the OAM order, the more resistant it is to fiber perturbations [2], [5], [6].

An RCF with a ring diameter of the same order of magnitude as the ring thickness is a good candidate for MIMO-free data transmission. Such a fiber was demonstrated in [3], where 12 spatial modes with a loss $\leqslant 1$ dB/km were received without MIMO-DSP over 1.2 km. Extending the number of modes is possible theoretically by increasing fiber index contrast. That has not been widely examined experimentally due to the difficulty and challenges in fabricating such fibers.

Multiplexers for OAM are still in the research stage; therefore, characterization, testing, and transmission experiments must rely on free-space setups [3], [7], [8]. Each OAM order has a different beam diameter and thickness. Hence, fiber coupling using lens assemblies is difficult to optimize. Perfect vortex (PV) beams [8] can modify the free-space OAM beam diameter and thickness. This technique has been used to launch OAM beams in RCF [8], [9], and efficiency was examined analytically in [10]. We use this technique for the measurement of mode-dependent loss (MDL). For the first time, to the best of our knowledge, we quantify the efficiency and purity of the PV beams using a mode-selective receiver; previous demonstrations [8], [9] relied on camera imaging.

Designing fiber with low MDL is crucial for MDM systems to maximize system capacity. Many techniques have been used to measure the modal loss: swept wavelength-interferometry (SWI) [11], optical time-domain reflectometry (OTDR) [12], and the conventional cutback technique. The SWI technique was used with low order OAM mode groups in [13] on RCF that was weakly guiding. The impact of multiplexers and demultiplexers is always present in the transfer matrix estimation [14]. Commercial OTDRs have standard single-mode fiber (SMF) input/output and require free-space selective mode launching [12] for MDL measurements. High Fresnel reflection at the fiber facet can saturate the OTDR detector [15], [16]. The saturation, combined with low back-scattered power at shorter fiber lengths, makes this method less accurate for OAM. The cutback technique is useful for short fiber lengths, but this technique is destructive. It is prohibitively wasteful of fiber when each mode supported calls for a separate round of measurements.

For core-cladding index difference below 2×10^{-2}, RCFs have shown loss below 1 dB/km and negligible MDL, that is, a difference of less than 0.1 dB/km across modes [12], [17]. On the other hand, RCFs with a higher core-cladding index difference [5], [18], [19], [20] have a loss above 2 dB/km and non-negligible differential loss. The high index contrast leads to an increase in Rayleigh scattering [21], [22] and fiber imperfections increase scattering loss at the ring-cladding interface, especially for higher-order modes [23].

Mai Banawan, Satyendra K. Mishra, Younès Messaddeq, Sophie LaRochelle and Leslie A. Rusch are with the Centre for Optics, Photonics and Lasers, Department of Electrical and Computer Engineering, Université Laval, Québec, QC, G1V 0A6, Canada (e-mail: mai.banawan.1@ulaval.ca; satyendra-kumar.mishra.1@ulaval.ca; younes.messaddeq@copl.ulaval.ca; sophie.larochelle@gel.ulaval.ca; rusch@gel.ulaval.ca). Mai Banawan is currently on leave from the Electrical Engineering Department, Alexandria University, Alexandria 21544, Egypt.

Manuscript received xx, 2022; revised xx, 2022.

Natural Sciences and Engineering Research Council of Canada (NSERC) Funding: CRDPJ515539

We fabricated a high-index contrast RCF proposed in [24]. Our RCF fiber supports modes up to order 13 and is, to the best of our knowledge, the highest number reported thus far (up to order 7 in [3] and up to order 9 in [18]). We take four fixed fiber lengths ranging from 10 m to 1.3 km to measure attenuation per mode in each fiber. Our loss estimate has the same accuracy as the conventional cutback technique with four data points; it is also non-destructive. The lower order modes are not typically targeted as they experience higher modal crosstalk (XT) as well as parasitic loss [20]. Higher-order modes can experience less coupling efficiency using free-space multiplexers. Therefore, we focus our attention on modal loss for orders 3 to 10. We proposed our method for the pseudo-cutback technique in [25]. In this paper, we extend our work and show in detail our method. We provide additional information on the fabricated fiber used in our experiments. We describe simulation and experimental optimization of beam width and diameter for mode excitation. We provide detailed time of flight traces to quantify the low multiplexer and demultiplexer XT. We provide an in-depth analysis of the limitations of OTDR methods for MDL estimation. We provide additional measurement data used in the estimation of the MDL.

The paper is organized as follows. In section II, we introduce the fabricated fiber. Section III presents our method for selective mode launch using PV beams and a programmable demultiplexer. We validate good selective excitation in section IV. In section V, we present our non-destructive MDL estimation technique and results for our fabricated fiber. Section VI is concluding remarks, followed by several appendices detailing our methodology.

II. RCF OAM Fiber Under Test

We fabricated the RCF design in [24], targeting transmission over 16 OAM channels, i.e., four OAM mode groups/orders. Further details on the fabricated fiber are given in Appendix A, including COMSOL simulations. We summarize some information here. In section IV, we present results on the MDL estimation using our non-destructive method.

We produced the preform via modified chemical vapor deposition (MCVD) with an inner core of fluorine-doped silica and a ring core of germanium-dioxide-doped silica. The cladding is pure silica, with a standard diameter of 125 μm. The measured fiber refractive index profile is given in Fig. 1(a) at 1550 nm. The inset is a radial projection that averages over all the angles, with a refractive index of 1.438 and 1.495 for the inner core and ring core, respectively. The high index difference of 5.1×10^{-2} between the ring-core and the cladding will limit the propagation distance of the fiber.

Appendix A presents complete simulation results on effective index separation and purity for all modes at 1550 nm. There are 118 eigenmodes that are guided at 1550 nm. Based on the simulated values, some OAM mode orders are expected to provide low enough XT for MIMO-free operation at a few kilometers of propagation.

We plot the simulated effective refractive index n_{eff} versus wavelength in Fig. 1(b) for the modes above order six. Using

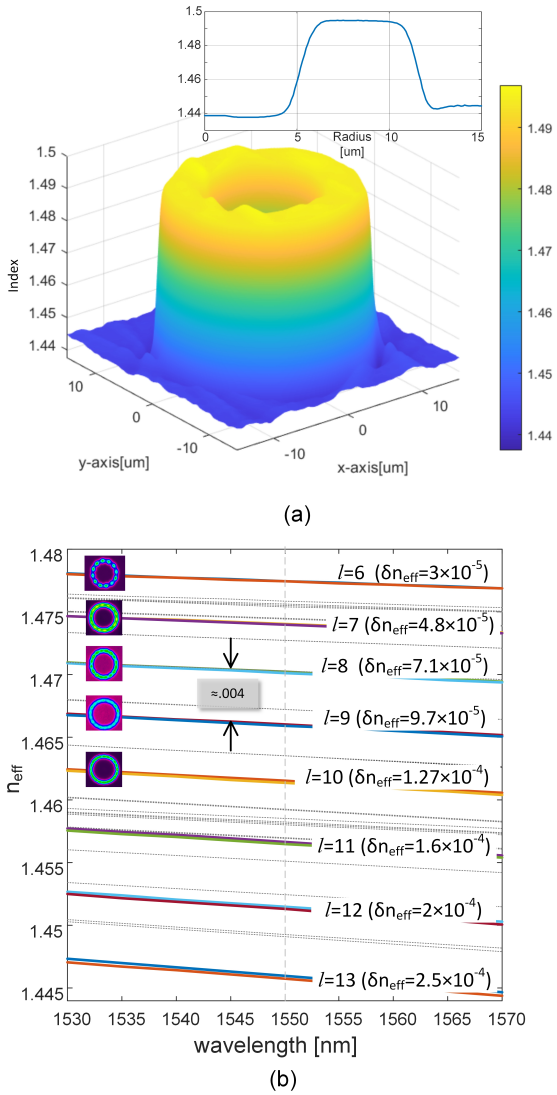

Fig. 1. (a) Measured index profile at 1550 nm with inset of radial projection (averaging over all angles), and (b) effective refractive index for selected OAM orders simulated from inset radial projection (grey dashed lines are non-targeted higher radial modes); images are experimental mode profiles after 1.3 km.

a charge-coupled device (CCD) camera in the setup described in section III, we recorded the intensity profiles after 1.3 km propagation. These images appear as insets in Fig. 1(b). The original fiber design targets modes 7 to 10 [24]. During fabrication, the doping concentration was higher than targeted, thus mode orders 11, 12, and 13 were also supported. However, these modes exhibited high coupling loss at the launch. As mode order increased, we saw the coupling loss grow in our free space setup; free-space divergence increases with mode order. Order 11 had coupling loss at the launch greater than 2 dB, hence, in the balance of the paper we consider only modes up to order 10.

An OAM fiber mode is a combination of two degenerate eigenmodes with circular polarization. Therefore, OAM modes come in degenerate pairs: spin-orbit aligned (A) and anti-aligned (AA) mode pairs [2], [18]. We see in Fig. 1(b) a very large separation between mode orders, Δn_{eff}, that grows

Natural Sciences and Engineering Research Council of Canada (NSERC) Funding: CRDPJ515539

with mode order. The separation gets larger as we progress to higher-order modes.

The effective index separation between A and AA modes, δn_{eff}, is considerably smaller, as indicated in the annotations in Fig. 1(b). While not visible in the plot, δn_{eff} also grows with mode order. The fiber is a good candidate for supporting up to four simultaneous mode groups for data transmission.

In general, higher mode orders would be preferred for data transmission due to their lower XT [2], [6]. In addition to XT, we must quantify the modal loss for a strategic choice of which modes to exploit.

III. Mode Selective Excitation and Detection

Our objective is to measure the modal loss per mode, which requires we launch a single OAM mode with high fidelity. We describe in subsection A how we find the optimal PV parameters to maximize coupling efficiency into the RCF. We describe in subsection B our re-programmable, free-space demultiplexer to estimate the modal content at the fiber output. In section IV, we will validate their performance.

A. Perfect Vortex Calibration

Our experimental setup is given in Fig. 2. The shaded box indicates the PV beam generation for any topological charge l. This setup allows us to adjust the diameter and thickness of the beam, i.e., the free-space OAM intensity ring. The better the match between the free-space mode and the RCF guided mode, the better the multiplexing performance we will achieve.

The zoom collimator lens (ZCL, Thorlabs ZC618FC-C) creates a Gaussian beam and is followed by a linear polarizer (LP). The polarization-sensitive spatial light modulator (SLM, Holoeye PLUTO, phase-only) is programmed to create the desired topological charge l. Per the technique in [8], the SLM forms a Bessel-Gauss beam. The 50 cm Fourier lens (FL) transforms the SLM output into a PV beam. A quarter-wave plate (QWP) changes the linearly polarized PV beam into circular polarization (for fiber transmission).

The zoom setting on the ZCL controls the Gaussian beam diameter ($2w_g$) across 1.07 to 3.27 mm. The larger the Gaussian beam, the thinner the intensity ring of the PV beam. The ring diameter is adjusted via the SLM using a spiral phase and axicon functions. The phase mask follows the argument of $\exp(iar + il\phi)$, for polar coordinates (r,ϕ) and a the axicon parameter [8]. The larger a, the larger the ring diameter of the PV beam. Experimentally, we use a molded glass aspherical lens from Thorlabs (A110TM-C with a focal length of 6.24 mm and 0.4 numerical aperture) to couple to the fiber. The detected power is measured to find the coupling efficiency.

We evaluate the coupling efficiency of the PV beams numerically and experimentally. Numerical simulations from theory are detailed in Appendix B. We report results here for $l = 8$, while appendix B shows results for all mode orders examined. We sweep (a, w_g) and plot the coupling efficiency in percentage using lighter tones for higher efficiency and darker tones for lower efficiency. In Fig. 3(a), results are simulated, while in Fig. 3(c), results are measured.

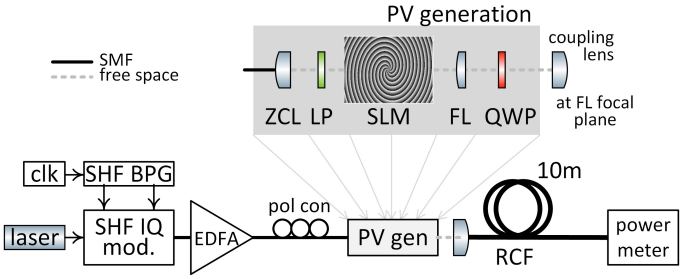

Fig. 2. Setup for Perfect Vortex (PV) generation and calibration using a modulated signal. The shaded box shows the setup to generate PV beams; zoom-collimator (ZCL), linear polarizer (LP), spatial light modulator (SLM), Fourier lens (FL), quarter wave-plate (QWP); bit pattern generator (BPG), In-phase and quadrature-phase (IQ) modulator, erbium-doped fiber amplifier (EDFA) and polarization controller (pol con)

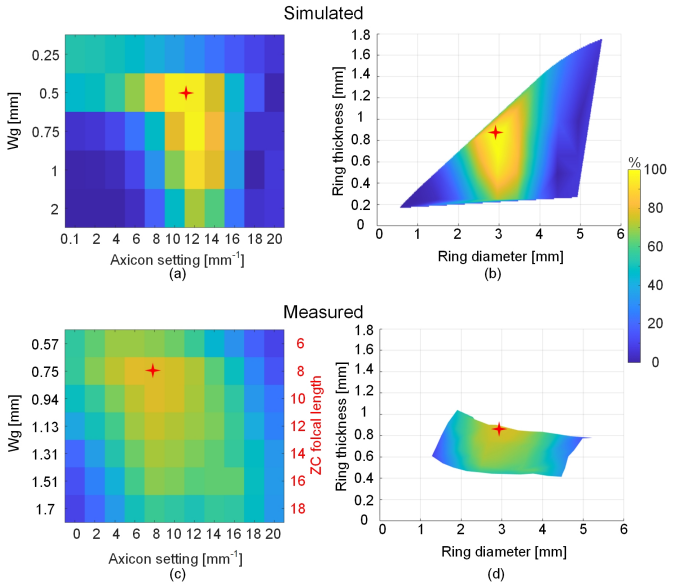

Fig. 3. Coupling efficiency for $l = 8$ as a function of axicon parameter a and Gaussian beam waist w_g in (a) as simulated, and (b) simulations replotted as a function of ring diameter and thickness, and (c) as measured and (d) measurements replotted as a function of ring diameter and thickness.

There is a one-to-one correspondence between ordered pairs (a, w_g) and (diameter, thickness) for the PV beam. The same results are re-plotted in Fig. 3(b) and (d) for simulated and measured results, respectively. Note that the PV beam diameter is defined as peak-to-peak axial intensity at the focusing lens (at the focal point of FL), while beam thickness is defined at $1/e^2$ of the intensity peak.

The crosses in Fig. 3 locate settings with the best coupling efficiency. Optimal coupling for simulated and measured results occur at identical beam diameter and thickness (3 mm and 1 mm, respectively). After focusing, this free-space beam profile is the closest match to the fiber mode profile. Optimal coupling occurs, however, at different values of (a, w_g) for the simulated and measured results. The discrepancy may come from the limitation of generating ideal Bessel-Gauss beams, especially for higher-order modes [26], or the need to calibrate the aspect ratio of SLM. We relied on experimental measurements to find the best SLM settings for each mode

Natural Sciences and Engineering Research Council of Canada (NSERC) Funding: CRDPJ515539

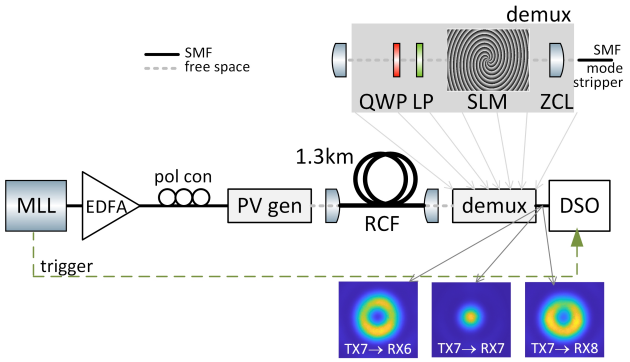

Fig. 4. Time of flight setup with a programmable demultiplexer (shaded box), and outputs for demux set to orders 6, 7 and 8 when launching order 7.

order (settings reported in Appendix B). These PV beams excite one mode at launch in all future experiments.

B. Demultiplexing

Our experimental setup is given in Fig. 4. The shaded box indicates the demultiplexer that can be programmed to isolate any topological charge l. The QWP converts the circularly polarized output OAM beam into linear polarization, which we align with the SLM active polarization.

For SLM programmed to receive l, input l is converted to fundamental, input $l+1$ is converted to order 1, input $l+2$ is converted to order 2, etc. The insets of image intensity in Fig. 4 are for projecting $l=7$. For the SLM programmed for $l=7$, we see a Gaussian profile. The energy at the center is coupled into an SMF. For the SLM programmed for $l=6$ or $l=8$, we see a ring profile. There is no energy at the center, so no light is coupled into an SMF, which acts as a mode stripper. When the input has XT, we would see some light at the center even for $l=6$ or $l=8$.

To verify the quality of the launch, we use a short fiber that will not introduce XT during propagation. The demultiplexer quantifies the XT induced by the multiplexer, i.e., the PV assembly. This is a finer measure than the coupling efficiency, which only measures total power on all modes.

IV. Validation of Mux and Demux

The modal loss will be obscured by all XT contributions. For a specific target mode, let M, D, and F be the percentage of power leaked to all the other modes by multiplexing, demultiplexing, and fiber propagation, respectively. When launching only the target mode, the received power on the target mode (P_T) and the received power on all other modes (P_o) are given by

$$\begin{bmatrix} P_T \\ P_o \end{bmatrix} = \begin{bmatrix} 1-D & D \\ D & 1-D \end{bmatrix} \times \begin{bmatrix} L_T & 0 \\ 0 & L_O \end{bmatrix} \times \begin{bmatrix} 1-F & F \\ F & 1-F \end{bmatrix} \times \begin{bmatrix} 1-M & M \\ M & 1-M \end{bmatrix} \times \begin{bmatrix} 1 \\ 0 \end{bmatrix} \tag{1}$$

A perfect estimate of the target modal loss requires that $M{=}D{=}F{=}0$, where L_T represents the remained power in the target mode after propagation loss.

In section IV-A, we will validate that M and F are indeed small for our setup and can be neglected. As D is found to be large at times, we will bypass the demultiplexer in modal loss estimates as in the conventional cutback method. In section IV-B, we turn from pulse characterization to measurement with a modulated signal to achieve higher power and more stable operation during loss estimation.

A. Time of Flight Measurements

When launching one mode in our RCF, we characterize the impulse response using time-of-flight (ToF) measurement with short pulses. This measurement allows us to distinguish between XT at launch/multiplexing (M), during propagation (F), and at the demultiplexer (D). The measurement can also quantify each contribution. As ToF allows us to identify modes by their unique propagation delays, we were able to verify that no measurable power was coupled to the OAM orders with multiple intensity rings.[1] Information on the propagation XT within one mode group of this fiber is examined with data transmission and coherent detection in [27].

As depicted in Fig. 4, a short impulse from a mode-locked laser (MLL) (Pritel, pulse width 3.5 ps with 3 nm filter) is amplified to 18 dBm by a Keopsys erbium-doped fiber amplifier (EDFA). The target PV beam is generated and traverses a short length of OAM RCF. After demultiplexing, a digital sampling oscilloscope (DSO) (Tektronix DSA8300 with 80 GHz optical bandwidth) captures the received signal. A trigger is used for synchronization.

We use the demultiplexer to collect traces for the target mode and one mode higher and lower than the target mode. Fig. 5 shows an example of ToF measurements for order 6 after 1.3 km of propagation. See Appendix C for ToF measurements for orders 3 to 10.

Figure 5a is the impulse response when the demultiplexer is programmed to the target mode. We observe some pulse broadening. The signal peak is at -30.9 dBm. We measured the pulse broadening at different fiber lengths and mode orders. We extract the modal dispersion and compare it with simulation results obtained from COMSOL (details in appendix E).

Figure 5b is the impulse response when the demultiplexer is programmed to one order lower, OAM5. This mode has a lower group delay than OAM6. In Fig. 5(b), we see a pre-cursor peak which we label mux; a small amount of OAM5 was inadvertently launched at the multiplexer and traveled faster than the main OAM6 pulse. We see another peak aligned with the arrival of the OAM6 pulse, which we label demux. The demultiplexer instantaneously coupled some of the received OAM6 to OAM5. The pedestal between these two peaks is due to power transfer between OAM5 and OAM6 during propagation, i.e., fiber XT.

In Fig. 5(b), the worst-case XT contribution is due to the multiplexer, with a peak power of -50 dBm. We adopt the shoulder-integration method as in [6] to calculate the fiber XT between the neighboring modes. The ratio of the shaded yellow area under the curve in Fig. 5(b) (shoulder) to the area

[1]These modes are considered parasitic as they are more difficult to couple and therefore not targeted for data communications.

Natural Sciences and Engineering Research Council of Canada (NSERC) Funding: CRDPJ515539

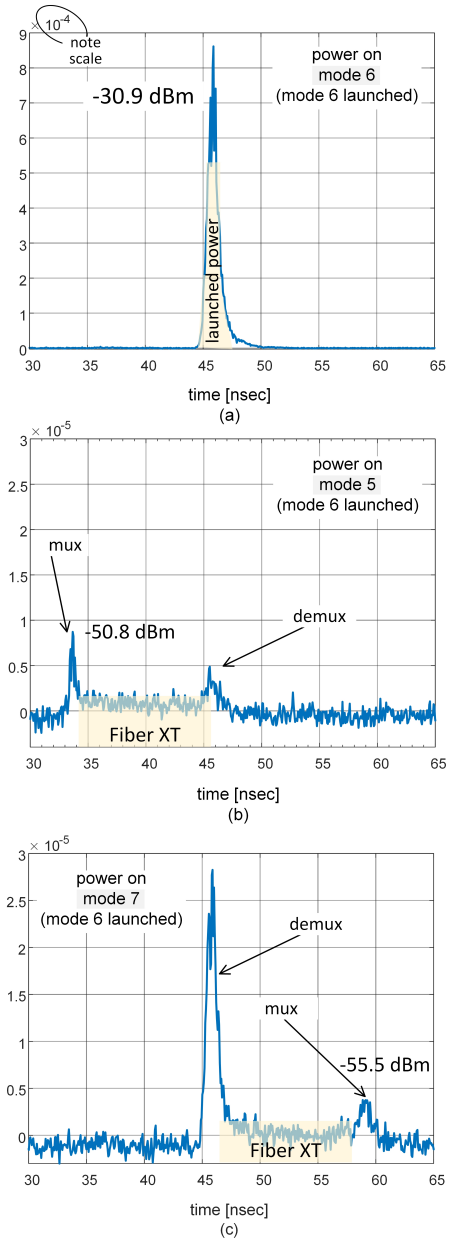

Fig. 5. Time of flight traces at 1.3 km giving power in mW, when launching AA on l=6 and setting the demultiplexer to (a) l=6, (b) l=5, and (c) l=7.

under the curve in Fig. 5(a) (main pulse) gives the fiber XT, which is under -20 dB. Note the scale change between the two plots. We conclude that M, F, and D are indeed negligible at 1.3 km. The worst-case total XT at the longest fiber examined was no worse than -12 dB for all the examined modes.

In Fig. 5(c), we receive the next highest mode, OAM7. As this mode has a larger group delay than OAM6, the demultiplexer XT peak precedes the multiplexer peak. We see that the worst-case XT contribution here is from the demultiplexer with a peak power of -45 dBm.

Following this type of measurement, we adopted the strategy of maintaining the demultiplexer for ToF validation of good launch. We removed the demultiplexer to estimate modal loss, essentially forcing D=0. The demultiplexer lets us see and quantify projections on the other modes than the launched mode but is not needed for loss estimation.

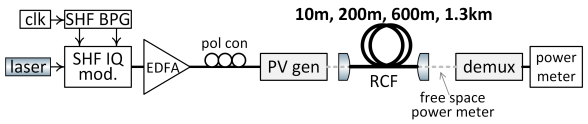

Fig. 6. Measurement setup using a modulated signal for modal loss measurement.

B. Modulated Signal Measurements

To quantify the fiber propagation loss, we turn to measurements with a modulated signal for higher power and more stable operation than MLL. As seen in the setup in Fig. 6, we bypass the demultiplexer and measure power with a free-space power meter. This assures $D = 0$. For each data point (fiber length), we use MLL with the demultiplexer to confirm a good launch. We then estimate modal loss with a modulated signal and no demultiplexer.

We generate 32 Gbaud quadrature phase-shift keying (QPSK) data using an SHF 12103A bit pattern generator with two pseudo-random binary sequences of lengths $2^{15}-1$ and $2^{20}-1$. The single polarization optical QPSK signal is created via an SHF46213D IQ modulator. We operate a Cobrite laser at 1550 nm with a linewidth of 100 kHz and with an output power of 10 dBm. A Keopsys EDFA amplifies the signal to 18 dBm.

The PV generator is programmed to launch each mode order l in turn into the fiber, from mode 3 to mode 10. One measurement is made for A modes l and one for the AA modes. In [25], we showed the recorded power after the demux for the launched mode and the neighboring modes using the setup in Fig. 6. These measurements summed all three XT contributions: M, F, and D, while ToF measurements, reported in the previous subsection, identify each contribution. The nearest neighbor modes remain more than 15 dB down from the target mode [25] for most of the total XT measurements with the modulated signal. Measurements are repeated for 10 m, 200 m, 600 m, and 1.3 km of fiber.

V. Nondestructive MDL Estimation

Two challenges exist for MDL estimation for RCF: 1) compromised accuracy due to accidental excitation of spurious modes, and 2) destruction of fiber that may be available only in limited quantities. In section V-A, we show that traditional OTDR techniques suffer from reduced accuracy. In section V-B, we propose a "pseudo-cutback" technique that is non-destructive. Four different lengths of fiber are reused for each individual modal excitation.

A. Traditional OTDR

We used an OTDR (Exfo FTB-7400B) with a dynamic range of 35 dB that operates at 1550 nm with a pulse width of 1 μs. We first launch into SMF-28e with known loss ($\leqslant$ 0.2 dB/km), with results seen in Fig. 8 in the grey dashed line. OTDR signal is launched to SMF-28e in free space using a collimating lens

Natural Sciences and Engineering Research Council of Canada (NSERC) Funding: CRDPJ515539

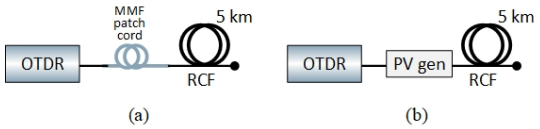

Fig. 7. OTDR setup with 5 km of fiber (a) with MMF and (b) with PV mode-selective excitation

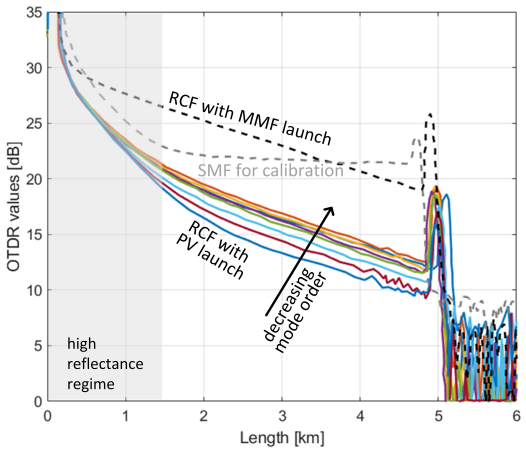

Fig. 8. OTDR traces: grey dashed curve for SMF launch, dark dashed curve for RCF launch with MMF path-cord, and colored curves for selective excitation of OAM3 to OAM10 using PV generation.

and coupling lens similar to those used in PV generator. We identified the region of high reflectance to be the first 1.3 km. Linear regression with a window size of 1 km along the OTDR trace after excluding this region gave a good prediction of the known loss.

Figure 7a is the setup we used to measure the general (not specific mode) loss as a baseline for comparison. We characterized 5 km of our RCF. We used a multimode fiber (MMF) patch-cord to increase the mode field diameter to accommodate the RCF. Lower-order modes are likely to be more excited as the OTDR launches the fundamental mode. The relative power launched in each mode is unknown. We can interpret this measurement as a statistical average of modal loss, but with very high variance and biased toward lower-order modes. We measured 2.25 dB/km fiber loss per the dark dashed line in Fig. 8.

We next used the PV generator to selectively excite modes with the OTDR launched pulse, as illustrated in Fig. 7(b). The back-scattered signal will pass through the PV generator before reaching the OTDR, this time acting as a demultiplexer for the launched mode. The PV generator (inset of Fig. 2) has a quarter-wave plate to change circular polarization to linear. Then, the backscattered light directly feeds the SLM. As it is polarization sensitive, only linearly polarized light on one axis will be demodulated by the SLM. The SLM then returns the desired mode order to the fundamental mode, and all other modes are stripped by the coupling into SMF. Inevitably, power will be lost from backscattered light with improper polarization, as well as loss from light scattering. This contributes to the weaknesses in the OTDR approaches.

In Fig. 8, we present in colored curves the OTDR traces for OAM3 to OAM10 averaged over 60 seconds. We observe more than a 7 dB drop in power using a mode-selective launch. The highest-order modes (9 and 10) approach the OTDR noise floor. For PV traces of order 3 to 8, we performed linear regression from 1.3 km to 3 km with a window size of 1 km. We estimated the modal loss as 2.3, 2.4, 2.5, 2.67, 2.7, and 3.2 dB/km for orders 3 to 8, respectively.

The estimate of modal loss was made up to 3 km, as data at longer distances was considered less reliable. For instance, the power received is lower at this distance, and there may be more mixing between different orders at a longer distance. The modal loss estimates also became less differentiated, with most modes having a loss of 2.5 dB/km.

B. Pseudo-Cutback Technique

The conventional fiber loss measurement is the cutback technique. Power is launched in a long fiber, and received power is measured at full length and is measured again following periodic cuts along the fiber length. The strength of this approach is that the launch conditions remain identical at each cut. For RCF supporting ten modes, ten fibers would need to be cut. For research into new RCF, the available amount of fiber could be limited. Given that fabrication techniques for RCF are still in evolution, variations may also occur at different fiber sections. Relying on multiple lengths of long fibers for MDL estimation may skew the characterization and hinder insights into improved designs and fabrication techniques.

In our pseudo-cutback technique, we take four fixed lengths of fiber ranging from 10 m to 1.3 km. For each fiber length, we excite each mode selectively in a round-robin fashion. By ensuring that launching XT is low, the estimated modal loss has the same accuracy as a cutback technique with four data points. Our technique is also non-destructive and more accurate than OTDR for these fiber lengths.

For launched power $P_T(0)$ on the target mode, the true mode loss after z km is given by

$$L_T(z) = \frac{P_T(z)}{P_T(0)} = 10^{-z \times m/10} \tag{2}$$

where $P_T(z)$ is the power received on the target mode alone and m is the modal loss in dB/km. In other words,

$$L_T(z)|_{dB} = -m \times z \tag{3}$$

Using the setup in Fig. 6, we measure free-space received power P_R. For each of the four fiber lengths, we launch a single polarization on the target mode. Results are given in Fig. 9 with one plot for each mode order, from OAM3 to OAM10. The markers indicate measurements are at 10 m, 200 m, 600 m, and 1.3 km, while the lines give the best linear fit of the four measurements.

The disparity in y-intercepts reflects the variation in coupling efficiency we achieved for the various modes. Per (3), the slope of each line can be used as an estimate, $\hat{m}$, for the modal loss in dB/km. Each plot has the loss estimation annotated, which we summarized in Table I, and we also summarized the MDL (differential loss) between each mode and the next

Natural Sciences and Engineering Research Council of Canada (NSERC) Funding: CRDPJ515539

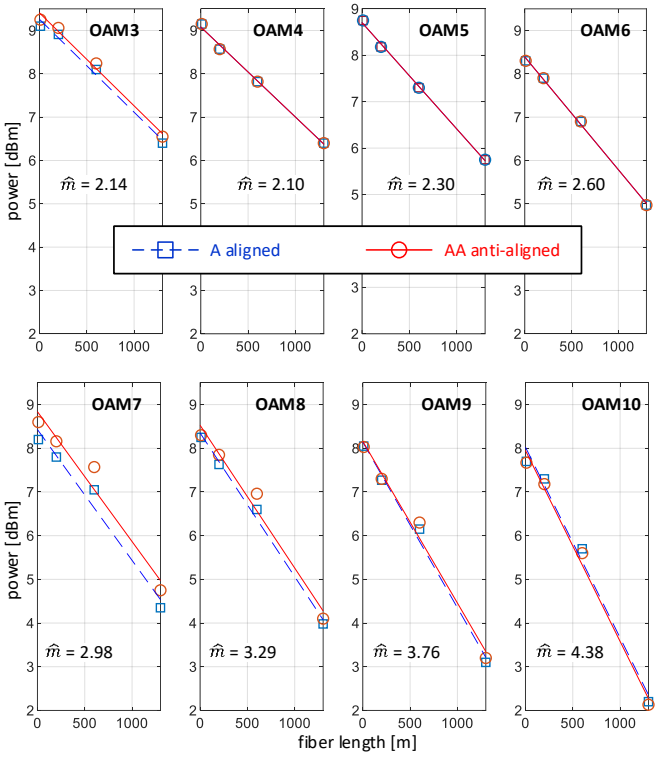

Fig. 9. Measured power for OAM3 to OAM10 at 10 m, 200 m, 600 m, and 1.3 km. Markers for measurements, lines for best linear fit, $\hat{m}$ in dB/km.

TABLE I: Estimated modal loss and MDL in dB/km using pseudo-cutback technique

l	3	4	5	6	7	8	9	10
$\hat{m}$ (dB/km)	2.14	2.1	2.3	2.6	2.98	3.29	3.76	4.38
MDL (dB/km)	0.0	0.2	0.3	0.38	0.31	0.47	0.62	-

neighboring mode order. Two factors influence the coupling efficiency: the mode field profile in the fiber and the free-space field at launch. The four fiber lengths were cut from a continuous length of fiber with fixed geometry, hence the field profile should be the same for all fiber lengths. The free-space field at launch was carefully monitored to assure uniformity. Our results summarize measurements repeated a few times on different days to assure we are getting the same power for each data collection. We did not observe many variations in power, as mux and demux XT were held low. As we can see in Fig. 9, the deviation between the linear fit and the measurements is not large. We are confident the changes in launching conditions are small. Most of the measurements show identical slopes for both A and AA modes. The highest disparity is for OAM3 and OAM7, and is less than 0.01 dB/km, indicating a small error in the measurements.

We observe the loss increases gradually with mode order. This is to be expected, as higher mode orders are more vulnerable to coupling to the cladding modes [28]. The MDL between successive orders (differential loss between them) also increases with mode order. Differential loss per km is 0 dB between orders 3 and 4. ; although not shown, we measured similar loss at orders 0, 1, and 2. The differential loss reaches 0.6 dB between orders 9 and 10. From the loss behavior, we expect orders 11 to 13 to have a modal loss > 4.38 dB/km.

The fiber loss is relatively high compared to other reported RCFs [4], [6], [17]. This is most likely due to the high index contrast, i.e., the index difference between the ring-core and the cladding. This was 5.1×10^{-2} for our fiber, and $\approx 8\times10^{-3}$ to 3×10^{-2} for fibers in [17], [4], [6].

Concerning the precision of the estimate, consider an estimate formed from two data points with a 1 km difference,

$$\begin{aligned}\hat{m} &= P_R(z_1)|_{dBm} - P_R(z_2)|_{dBm} = \left.\frac{P_R(z_1)}{P_R(z_2)}\right|_{dB} \\ &= \left.\frac{P_T(z_1)+P_o(z_1)}{P_T(z_2)+P_o(z_2)}\right|_{dB} \\ &= \left.\frac{P_T(z_1)}{P_T(z_2)}\right|_{dB} + \left.\frac{1+XT(z_1)}{1+XT(z_2)}\right|_{dB} \\ &= m + \left.\frac{1+XT(z_1)}{1+XT(z_2)}\right|_{dB} \leq m \pm [1+XT_{wc}]_{dB}\end{aligned} \tag{4}$$

where $XT(z) = P_o(z)/P_T(z)$ is the cumulative XT at length z and XT_{wc} is the worst case cumulative XT. This gives a loose upper bound on the accuracy of the estimates. In most cases, the cumulative XT in both numerator and denominator would be comparable, with somewhat more XT at longer distances. Our worst-case cumulative XT was -17 dB, corresponding to ±0.086 dB. Note this XT figure has a contribution from the multiplexer and fiber but not demultiplexer as we bypassed it.

VI. Conclusion

We fabricated a high-index-contrast RCF that supports many OAM mode orders, and we report results for eight modes. We characterized the modal loss using a nondestructive modified cut-back technique. We employed mode selective excitation using PV beams with high coupling efficiency and low multiplexer XT. Before each measurement on a single mode, a ToF experiment with a free-space demultiplexer validated low XT. A modulated signal with high power was then used to measure the modal loss.

We quantified the modal loss for eight OAM mode orders, or 16 OAM mode pairs (A and AA pairs). Traditional cutback methods would have consumed a fiber for each characterization. The modal loss was found to increase with mode order, first slowly, then steeply. Little difference was found in the modal loss between A and AA modes in the same mode group. Two OTDR methods yielded MDL estimates that significantly underestimated the differential loss across modes 3 to 10. For OTDR without selective excitation, there was zero differential loss. For OTDR with mode-selective excitation, low received backscattered power and limitations due to high Fresnel reflectance led to estimates of MDL spanning 2.3 to 3.2 dB/km for orders 3 to 8 while the loss for higher-order modes could not be measured. Our method led to estimates with a greater differential, i.e., spanning 2.14 to 4.38 dB/km for modes 3 to 10.

Natural Sciences and Engineering Research Council of Canada (NSERC) Funding: CRDPJ515539

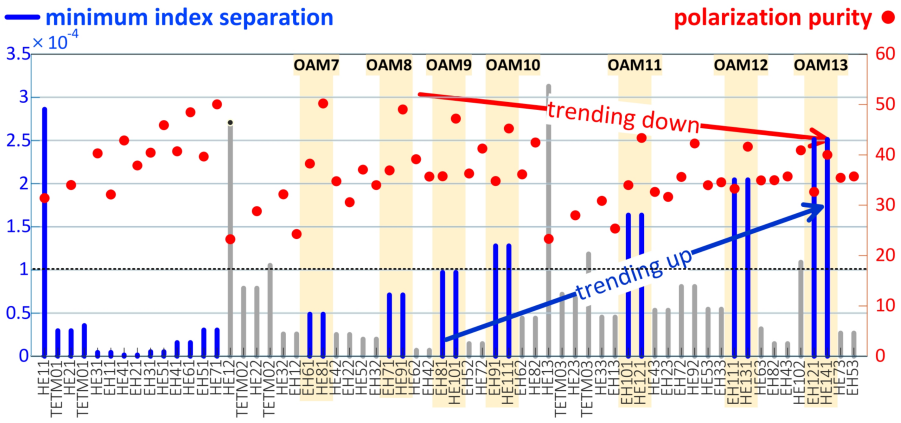

Fig. 10. Minimum index separation (bars, left axis) and mode purity (dots, right axis) for all eigenmodes at 1550 nm. Grey data is for OAM modes with multiple intensity rings. Boxes highlight OAM modes with best prospects for low XT.

Appendix A
Simulation of Fabricated Fiber

Our COMSOL simulation was exploited to find two important figures of merit contributing to XT behavior: the minimum effective index separation between modes and the purity. These are defined and calculated as in [24]. In Fig. 10, the two figures of merit are presented on one plot. The x-axis specifies the eigenmode. The left axis and blue bars indicate minimum effective index separation (i.e., separation with the nearest eigenmode), while the right axis and red dots indicate modal purity in dB.

Each OAM mode is a combination of two fiber eigenmodes: HE eigenmodes contribute to the aligned (A), and EH eigenmodes contribute to the anti-aligned (AA) mode as in [2]. Each OAM mode has a dominant component with order l and a secondary component with order $l\pm2$ in the opposite circular polarization [2], [24]. The power ratio of the components defined the polarization mode purity in Fig. 10.

While the fabricated fiber supports 118 eigenmodes guided at 1550 nm, this includes modes of multiple intensity rings. Those modes are more difficult to couple efficiently into the fiber and will not be exploited for data communications. For several modes with single intensity rings, we have drawn shaded boxes in Fig. 10 around the modes contributing to one OAM order and added annotation of the OAM order. Modes with multiple intensity rings have an effective index separation, shown in light grey.

The blue upward trending line in Fig. 10 highlights that higher-order modes have larger intra-modal separations δn_{eff}. The dotted line is a rule of thumb threshold on δn_{eff} for predicting low XT as proposed in [24]. Mode order 9 and above meet the threshold, and mode 8 is near. Although the modal purity is trending down for the higher-order modes, modal purity is still high for our RCF compared to fiber with a small thickness [24]. The purity for the highest mode was $>$ 30 dB, while the thin fiber in [24] had a purity $<$ 20 dB. Hence, the effect of spin-orbit coupling is expected to be small in our fiber, and we will not need to launch non-integer OAM modes to overcome this coupling [29]. An experimental investigation is needed to see how these two factors, and others, will enter into play to determine the lowest XT modes. For instance, mode orders 11 to 13 have fast divergence in free space, and it was challenging to couple them efficiently into the fiber.

TABLE II: Effective mode area and macro-banding loss for a 1 cm bending radius

l	3	4	5	6	7	8	9	10
A_{eff} (μm^2)	241.78	244.47	246.62	244.85	241.53	237.29	232.72	228.22
Macro-bending loss (dB/km)	7.4E-07	1.6E-07	6.6E-08	8.3E-07	7.8E-07	2.1E-07	1.4E-05	1.3E-04

We calculate the effective mode area (A_{eff}) and macro-bending loss as in [19] for orders 3 to 10 and report them in Table II. As A_{eff} is always greater than $>$ $228\mu m^2$, this is sufficient to avoid nonlinear effects in short-reach communications. The macro-bending loss was calculated for a 1 cm bending radius and is small. In our experiment, we wind the fiber on a spool with a large diameter of 30 cm and avoid any loss from macro-bending.

Appendix B
Details on Perfect Vortex Generation

We predict the beam diameter and width numerically for optimal coupling efficiency. We simulate the setup for generating PV beams in the dashed box in Fig. 2. Bessel-Gauss beam, generated using the SLM (see equation (5) in [8]), will propagate in free space before passing through the Fourier-lens. The free-space propagation is modeled in MATLAB using Rayleigh-Sommerfeld diffraction [30]. Fourier-lens is simulated as a spherical thin lens with a 50 cm focal length. The beam will propagate 50 cm in the free space to form the PV beam before coupling into the fiber. The 6.24 mm focusing lens is also modeled as a spherical thin lens. The beam will propagate in the free space to the fiber input facet. We calculate the overlap integral between the fiber modes (calculated using COMSOL as described in section II) and the free-space beam at the fiber facet. We swept a and w_g, which will change the Bessel-Gauss beam generated by the SLM, to find the optimal coupling efficiency in Fig. 3 (a) and (b).

Natural Sciences and Engineering Research Council of Canada (NSERC) Funding: CRDPJ515539

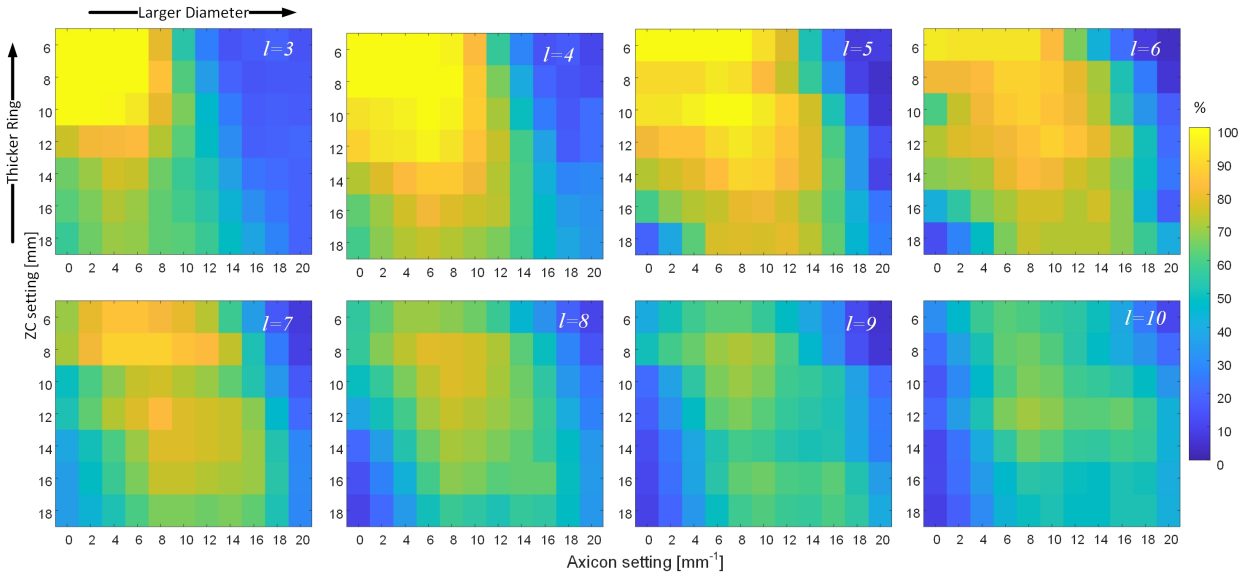

Fig. 11. Coupling efficiency (as a percentage) for orders 3 to 10, axicon parameter a is swept from 0 to 20/mm to increase free-space beam diameter, ZCL setting (controlling w_g) is swept from 6 mm to 18 mm to decrease ring thickness with increasing w_g. higher-order modes require smaller thickness and larger diameter compared to lower-order modes

We swept a and w_g experimentally to confirm previous results. We use the setup in the dashed box in Fig. 2. Light is coupled into 10 m of RCF. Power at the input facet of the fiber is 10 dBm. We defined the experimental coupling efficiency as the ratio (in percentage) of power coupled into 10 m of RCF fiber to the power at the input facet of the fiber. Results are plotted in Fig. 3 (c). We found some discrepancies between the optimal value for a achieved experimentally (8/mm) in Fig. 3 (c) and the numerical value (12/mm) in Fig. 3 (a). However, the corresponding optimal beam diameter and width achieved experimentally and shown in Fig. 3 (d) matches the numerical optimal beam diameter and width in Fig. 3 (b).

Similar to order 8, we swept a and ZCL setting to find the optimal PV beam diameter and width. Results for topological charge (3 to 10) are in Fig. 11. The settings are distinct from lower to higher-order modes, as shown in Table III. Lower-order mode (e.g., $l = 3$) requires a small free-space beam diameter (a is less than 4/mm) while higher-order mode (e.g., $l = 10$) needs a relatively large beam diameter (a is around 8/mm) and ZCL setting of $f = 12mm$. As shown in Fig. 11 and Table III, the maximum coupling efficiency decreases with increasing topological charge due to the high divergence of the free space beam of higher mode order. For $l > 10$, the minimum coupling loss was >2 dB. Changing the focusing lens to a higher numerical aperture can improve the coupling efficiency. For our available focusing lenses, we choose to characterize up to $l = 10$. The behavior of higher-order modes can be predicted. Balancing the excess loss will be required for data transmission experiments.

Appendix C
ToF Nearest Neighbor Measurements

We measured the ToF for orders 3 to 10 using the setup in Fig. 4 for different fiber lengths. Results for 1.3 km are shown in Fig. 12. For each order l, we plot the impulse response when receiving the desired mode l (in red) and when receiving the two neighboring modes $l \pm 1$ (in blue). The average over many captured traces is plotted to suppress the noise. We wrote the power level of the impulse peak in dBm at the arrival time of each mode. These levels indicate the excitation purity of each mode. We observe that each mode is launched by at least 20 dB from the neighboring modes, which is sufficient for loss measurement.

TABLE III: Optimal settings and performance

l	3	4	5	6	7	8	9	10
Minimum coupling loss (dB)	0	0	0	0.2	0.4	0.9	1.4	1.6
Axicon setting (/mm)	2	4	6	6	6	6	8	8
ZCL setting (mm)	6	6	6	6	8	8	8	12

From the ToF measurement, fiber XT appears as a power distribution between two mode groups (shaded in yellow in Fig. 12). The measured XT between nearest neighbors varies between -18.6 dB to -21 dB for $l = 3$ to 10.

Appendix D
Dispersion

In Fig. 12, the pulse broadening increases with mode order, while A/AA mixing decreases with increasing mode order [2], [6], [24]. Therefore, the broadening is not coming from coupling [31] but rather from chromatic dispersion [6]. We calculate fiber dispersion from the COMSOL results [32]. Simulated fiber dispersion is shown in Fig. 13(a) and grows with mode order. From ToF traces, the full-width half maximum (FWHM) pulse width is plotted against fiber length in Fig. 13(b).

The pulse broadening from chromatic dispersion is $dL\Delta\lambda$ [32], where d is the fiber dispersion, L is the fiber length, and

Natural Sciences and Engineering Research Council of Canada (NSERC) Funding: CRDPJ515539

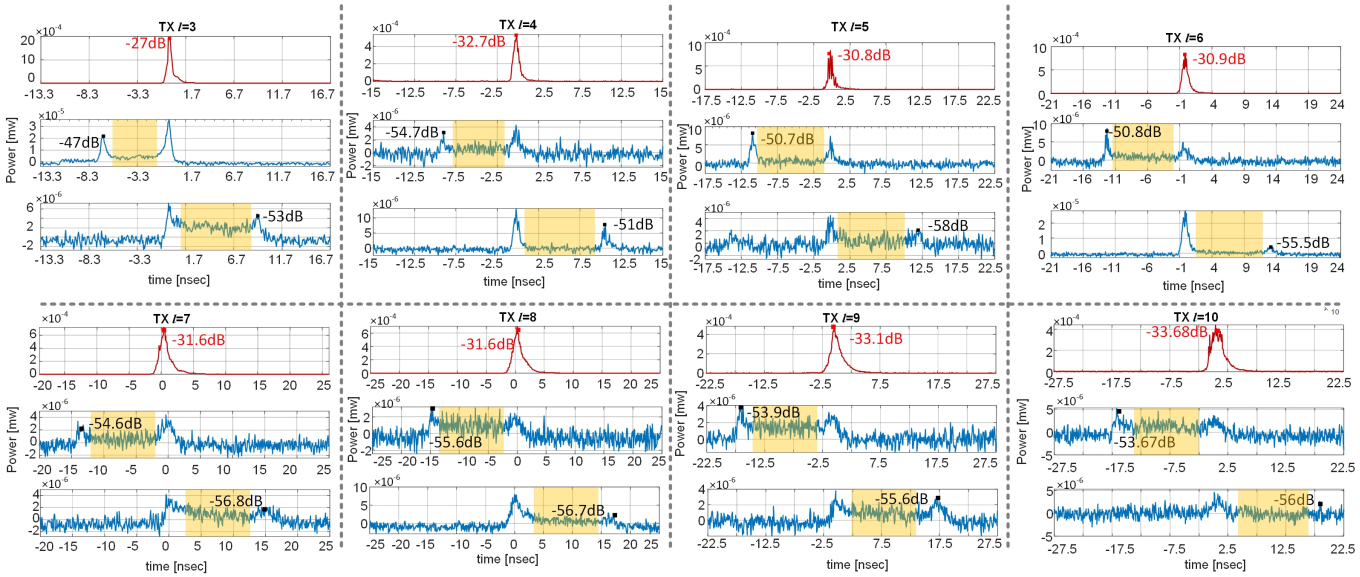

Fig. 12. ToF measurements for l=3 to 10 after 1.3 km of fiber using the setup in Fig. 4 for launching order l. Impulse response when receiving launched mode (l) is plotted in red and blue impulse responses when receiving two neighboring modes ($l \pm 1$). Peak launch power at fiber input is indicated for each trace, revealing a good launch of the desired mode. The shaded yellow region indicates low in-fiber inter-modal XT.

$\Delta\lambda$ is the spectral width of the optical pulse. The slopes in Fig. 13(b) are $d\Delta\lambda$.

We measured the spectral width of the amplified pulse from MLL in Fig. 4 with optical spectrum analyzer. The spectral width of the pulse was around 10 nm, which resulted in a highly dispersed pulse. The measured fiber dispersion can be estimated as 36, 47, 54.7, 69, 91, 105.6, 130, and 143 ps/(nm.km) for orders 3 to 10, respectively. The calculated dispersion from the measured ToF agrees with the simulation results. The large increase in the spectral bandwidth confirms that self-phase modulation effects are not negligible in our setup, as discussed in [6]. We need to carefully avoid this effect, especially when examining intra-mode XT.

Acknowledgement

We would like to thank Nathalie Bacon for her assistance and knowledgeable advice on the experimental setup.

Funding

This work was supported in part by Huawei Canada and in part by Natural Sciences and Engineering Research Council of Canada (NSERC) under Grant CRDPJ515539. This work is part of the research program of the Canada Research Chair on Communications Systems Enabling the Cloud.

References

[1] N. Bozinovic, Y. Yue, Y. Ren, M. Tur, P. Kristensen, H. Huang, A. E. Willner, and S. Ramachandran, "Terabit-scale orbital angular momentum mode division multiplexing in fibers," *Science*, vol. 340, no. 6140, pp. 1545–1548, 2013.

[2] M. Banawan, L. Wang, S. LaRochelle, and L. A. Rusch, "Quantifying the coupling and degeneracy of OAM modes in high-index-contrast ring core fiber," *Journal of Lightwave Technology*, vol. 39, no. 2, pp. 600–611, 2020.

[3] K. Ingerslev, P. Gregg, M. Galili, F. Da Ros, H. Hu, F. Bao, M. A. U. Castaneda, P. Kristensen, A. Rubano, L. Marrucci *et al.*, "12 mode, WDM, MIMO-free orbital angular momentum transmission," *Optics express*, vol. 26, no. 16, pp. 20 225–20 232, 2018.

[4] R. M. Nejad, K. Allahverdyan, P. Vaity, S. Amiralizadeh, C. Brunet, Y. Messaddeq, S. Larochelle, and L. A. Rusch, "Mode Division Multiplexing Using Orbital Angular Momentum Modes over 1.4-km Ring Core Fiber," *Journal of Lightwave Technology*, vol. 34, no. 18, pp. 4252–4258, 2016.

[5] P. Gregg, P. Kristensen, and S. Ramachandran, "Conservation of orbital angular momentum in air-core optical fibers," *Optica*, vol. 2, no. 3, pp. 267–270, 2015.

[6] ——, "13.4 km OAM state propagation by recirculating fiber loop," *Optics express*, vol. 24, no. 17, pp. 18 938–18 947, 2016.

[7] J. Liu, G. Zhu, J. Zhang, Y. Wen, X. Wu, Y. Zhang, Y. Chen, X. Cai, Z. Li, Z. Hu *et al.*, "Mode division multiplexing based on ring core optical fibers," *IEEE Journal of Quantum Electronics*, vol. 54, no. 5, pp. 1–18, 2018.

[8] P. Vaity and L. Rusch, "Perfect vortex beam: Fourier transformation of a bessel beam," *Optics letters*, vol. 40, no. 4, pp. 597–600, 2015.

[9] G. Zhu, Y. Chen, Y. Liu, Y. Zhang, and S. Yu, "Characterizing a 14x14 OAM mode transfer matrix of a ring-core fiber based on quadrature phase-shift interference," *Optics Letters*, vol. 42, no. 7, pp. 1257–1260, 2017.

[10] S. Rojas-Rojas, G. Cañas, G. Saavedra, E. S. Gómez, S. P. Walborn, and G. Lima, "Evaluating the coupling efficiency of OAM beams into ring-core optical fibers," *Optics Express*, vol. 29, no. 15, pp. 23 381–23 392, 2021.

[11] K. F. Nicolas, "Characterization of multi-mode fibers and devices for MIMO communications," in *Proc.SPIE*, vol. 9009, Conference Proceedings. [Online]. Available: https://doi.org/10.1117/12.2044339

[12] Y. Jung, Q. Kang, H. Zhou, R. Zhang, S. Chen, H. Wang, Y. Yang, X. Jin, F. P. Payne, S.-u. Alam *et al.*, "Low-loss 25.3 km few-mode ring-core fiber for mode-division multiplexed transmission," *Journal of Lightwave Technology*, vol. 35, no. 8, pp. 1363–1368, 2017.

[13] J. Zhang, J. Zhu, J. Liu, S. Mo, J. Zhang, Z. Lin, L. Shen, L. Zhang, J. Luo, J. Liu *et al.*, "Accurate mode-coupling characterization of low-crosstalk ring-core fibers using integral calculation based swept-wavelength interferometry measurement," *Journal of Lightwave Technology*, vol. 39, no. 20, pp. 6479–6486, 2021.

[14] H. Chen, N. K. Fontaine, and R. Ryf, "Transfer matrix characterization of 10-mode mode-selective spatial multiplexers," in *2016 IEEE Photonics Society Summer Topical Meeting Series (SUM)*, Conference Proceedings, pp. 51–52.

[15] M. Nakazawa, M. Yoshida, and T. Hirooka, "Measurement of mode coupling distribution along a few-mode fiber using a synchronous multi-channel OTDR," *Optics Express*, vol. 22, no. 25, pp. 31 299–31 309, 2014.

[16] Z. Wang, H. Wu, X. Hu, N. Zhao, Q. Mo, and G. Li, "Rayleigh scattering

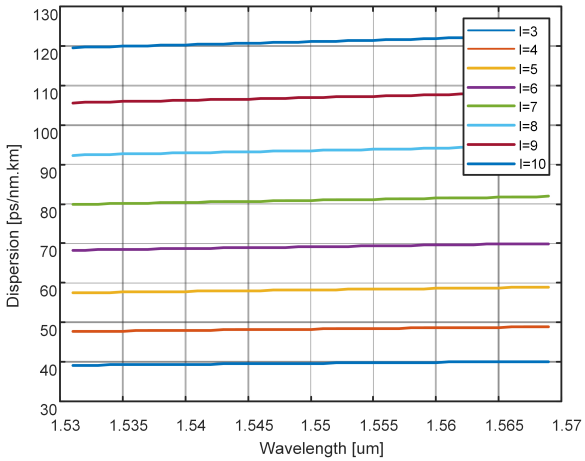

(a)

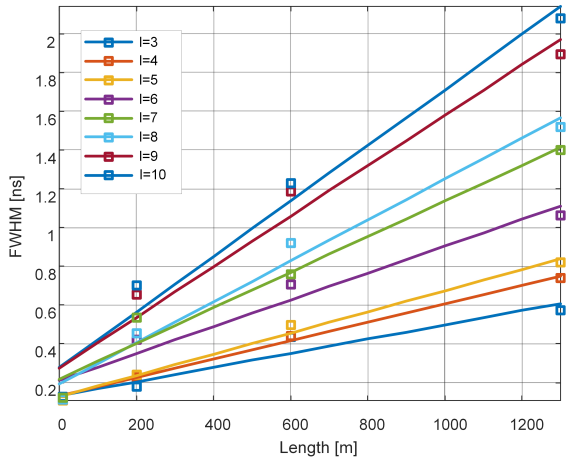

(b)

Fig. 13. (a) Dispersion vs. wavelength for orders 3 to 10, calculated from COMSOL results (modal group index) and (b) pulse broadening for orders 3 to 10 calculated from ToF traces using the setup in Fig. 4 for different lengths, slope depends on modal dispersion and spectral width of launched impulse.

in few-mode optical fibers," *Scientific reports*, vol. 6, no. 1, pp. 1–8, 2016.

[17] J. Zhang, J. Liu, L. Shen, L. Zhang, J. Luo, J. Liu, and S. Yu, "Mode-division multiplexed transmission of wavelength-division multiplexing signals over a 100-km single-span orbital angular momentum fiber," *Photonics Research*, vol. 8, no. 7, pp. 1236–1242, 2020.

[18] C. Brunet, P. Vaity, Y. Messaddeq, S. LaRochelle, and L. A. Rusch, "Design, fabrication and validation of an OAM fiber supporting 36 states," *Optics express*, vol. 22, no. 21, pp. 26 117–26 127, 2014.

[19] B. Ung, P. Vaity, L. Wang, Y. Messaddeq, L. Rusch, and S. LaRochelle, "Few-mode fiber with inverse-parabolic graded-index profile for transmission of OAM-carrying modes," *optics express*, vol. 22, no. 15, pp. 18 044–18 055, 2014.

[20] R. M. Nejad, L. Wang, J. Lin, S. LaRochelle, and L. A. Rusch, "The impact of modal interactions on receiver complexity in OAM fibers," *Journal of Lightwave Technology*, vol. 35, no. 21, pp. 4692–4699, 2017.

[21] K. Tsujikawa, K. Tajima, and J. Zhou, "Intrinsic loss of optical fibers," *Optical Fiber Technology*, vol. 11, no. 4, pp. 319–331, 2005.

[22] M. E. Likhachev, M. M. Bubnov, S. L. Semenov, V. V. Shvetsov, V. F. Khopin, A. N. Gur'yanov, and E. M. Dianov, "Mechanisms of optical losses in fibres with a high concentration of germanium dioxide," *Quantum Electronics*, vol. 33, no. 7, p. 633, 2003.

[23] M. Bsaibes, Y. Quiquempois, S. Plus, A. Masselot, G. Labroille, M. Bigot-Astruc, J.-B. Trinel, P. Sillard, and L. Bigot, "Light scattering mechanisms in few-mode fibers," *Journal of Lightwave Technology*, 2022.

[24] J. H. Chang, A. Corsi, L. A. Rusch, and S. LaRochelle, "Design analysis of OAM fibers using particle swarm optimization algorithm," *Journal of Lightwave Technology*, vol. 38, no. 4, pp. 846–856, 2019.

[25] M. Banawan, S. K. Mishra, S. LaRochelle, and L. A. Rusch, "Modal loss characterisation of thick ring core fiber using perfect vortex beams," in *2022 Optical Fiber Communications Conference and Exhibition (OFC)*. IEEE, 2022, pp. 1–3.

[26] J. Arlt and K. Dholakia, "Generation of high-order bessel beams by use of an axicon," *Optics Communications*, vol. 177, no. 1-6, pp. 297–301, 2000.

[27] M. Banawan, S. K. Mishra, A. Gouin, N. Bacon, X. Guan, L. Wang, S. LaRochelle, and L. A. Rusch, "Expanded modal capacity for OAM with standard 2×2 MIMO," in *2022 European Conference on Optical Communication (ECOC)*. IEEE, 2022, pp. 1–4.

[28] X. Jin, A. Gomez, K. Shi, B. C. Thomsen, F. Feng, G. S. Gordon, T. D. Wilkinson, Y. Jung, Q. Kang, P. Barua *et al.*, "Mode coupling effects in ring-core fibers for space-division multiplexing systems," *Journal of Lightwave Technology*, vol. 34, no. 14, pp. 3365–3372, 2016.

[29] P. Gregg, P. Kristensen, A. Rubano, S. Golowich, L. Marrucci, and S. Ramachandran, "Enhanced spin orbit interaction of light in highly confining optical fibers for mode division multiplexing," *Nature communications*, vol. 10, no. 1, pp. 1–8, 2019.

[30] D. G. Voelz, *Computational fourier optics: a MATLAB tutorial*. SPIE press Bellingham, WA, 2011.

[31] R. Maruyama, N. Kuwaki, S. Matsuo, and M. Ohashi, "Relationship between mode coupling and fiber characteristics in few-mode fibers analyzed using impulse response measurements technique," *Journal of Lightwave Technology*, vol. 35, no. 4, pp. 650–657, 2016.

[32] G. P. Agrawal, *Fiber-optic communication systems*. John Wiley & Sons, 2012, vol. 222.

Natural Sciences and Engineering Research Council of Canada (NSERC) Funding: CRDPJ515539